SAND REPORT
SAND 2003-8666
Unlimited Release
Printed November 2003

Development of Detection Techniques and Diagnostics for Airborne Carbon Nanoparticles

H. A. Michelsen, P. O. Witze, T. B. Settersten

Prepared by
Sandia National Laboratories
Albuquerque, New Mexico 87185 and Livermore, California 94550

Sandia is a multiprogram laboratory operated by Sandia Corporation, a Lockheed Martin Company, for the United States Department of Energy under Contract DE-AC04-94AL85000.

Sandia National Laboratories

Issued by Sandia National Laboratories, operated for the United States Department of Energy by Sandia Corporation.

Available to DOE and DOE contractors from
U.S. Department of Energy
Office of Scientific and Technical Information
P.O. Box 62
Oak Ridge, TN 37831

Telephone: (865)576-8401
Facsimile: (865)576-5728
E-Mail: reports@adonis.osti.gov
Online ordering: http://www.osti.gov/bridge

Available to the public from
U.S. Department of Commerce
National Technical Information Service
5285 Port Royal Rd
Springfield, VA 22161

Telephone: (800)553-6847
Facsimile: (703)605-6900
E-Mail: orders@ntis.fedworld.gov
Online order: http://www.ntis.gov/ordering.htm

SAND2003-8666
Unlimited Release
Printed November 2003

Development of Detection Techniques and Diagnostics for Airborne Carbon Nanoparticles

H. A. Michelsen
Diagnostics and Remote Sensing Department

P. O. Witze
Engine Combustion Department

T. B. Settersten
Diagnostics and Remote Sensing Department

Sandia National Laboratories
MS 9055
P. O. Box 969
Livermore, CA 94551

Abstract

We have recorded time-resolved LII signals from a laminar ethylene diffusion flame over a wide range of laser fluences at 532 nm. We have performed these experiments using an injection-seeded Nd:YAG laser with a pulse duration of 7 ns. The beam was spatially filtered and imaged into the flame to provide a homogeneous spatial profile. These data were used to aid in the development of a model, which will be used to test the validity of the LII technique under varying environmental conditions. The new model describes the heating of soot particles during the laser pulse and the subsequent cooling of the particles by radiative emission, sublimation, and conduction. The model additionally includes particle heating by oxidation, accounts for the likelihood of particle annealing, and incorporates a mechanism for nonthermal photodesorption, which is required for good agreement with our experimental results.

In order to investigate the fast photodesorption mechanism in more detail, we have recorded LII temporal profiles using a regeneratively amplified Nd:YAG laser with a pulse duration of 70 ps to heat the particles and a streak camera with a temporal resolution of ~65 ps to collect the signal. Preliminary results confirm earlier indications of a fast mechanism leading to signal decay rates of much less than a nanosecond.

Parameters to which the model is sensitive include the initial soot temperature, the temperature of the ambient gas, and the partial pressure of oxygen. In order to narrow the model uncertainties, we have developed a source of soot that allows us to determine and control these parameters. Soot produced by a burner is extracted, diluted, and cooled in a flow tube, which is equipped with a Scanning Mobility Particle Sizer (SMPS) for characterization of the aggregates.

Acknowledgments

We thank B. Axelsson, D. Kayes, S. Hochgreb, C. R. Shaddix, W. L. Hsu, R. M. Green, and D. A. V. Kliner for enlightening discussions, insightful comments, and helpful suggestions. This work was supported by the Division of Chemical Sciences, Geosciences, and Biosciences, Office of Basic Energy Sciences, U. S. Department of Energy, and the Sandia Laboratory Directed Research and Development Program.

Contents

Figures

Introduction

Newer generation Compression Ignition Direct Injection (CIDI) diesel engines, which have been designed for low particulate-matter mass emissions, emit no visible soot, but they may generate far greater numbers of small particles than older diesel engines.[1] Hybrid cars incorporating CIDI engines are expected to be commercially available in the US by the year 2004. New evidence strongly suggests that gasoline engines also emit large numbers of small particles under some operating conditions.[1] These small (sub-micron) particulates are classified as a toxic emission in California, may pose a greater health risk than larger soot particles,[2,3] and are expected to have a significant impact on the Earth's climate.[4] Emissions of small particulate are thus of emerging concern.

Combustion-generated soot particles consist of fractal-like, branched-chain aggregates of small (5-50 nm diameter) carbon spheroids called primary particles. Soot particles emitted by diesel engines are coated with unburned fuel, sulfate, water, and other combustion by-products.[1] The non-spherical shapes and inhomogeneous compositions of these aggregate particles make measurements of their size difficult, particularly if fast time response and high sensitivity to small particles are required. Traditional methods for sampling engine emissions using gravimetric analysis, tapered element oscillating microbalances, and smoke meters have slow response times and low sensitivities to sub-micron particles. The scanning mobility particle sizer (SMPS) is sensitive to fine particles but requires dilution of the exhaust stream, which can lead to significant changes in particle characteristics. Common optical techniques, on the other hand, have fast response times and are non-invasive but are either not sensitive enough to fine particles (single-pass extinction) or are highly complex (angle- and polarization-resolved light scattering). Laser-induced incandescence (LII) is a possible sensitive alternative optical technique that is relatively simple to implement, but the conditions under which this technique can provide quantitative volume fraction measurements have not been established.

LII involves heating the soot particles by laser irradiation to temperatures (2500-4500 K) at which they incandesce (i.e., emit observable blackbody radiation) and detecting the emitted light. The rates of absorption of the laser light and emission of incandescence are generally assumed to be linearly dependent on particle volume fraction.[5-8] LII has been used extensively to measure volume fractions and image spatial distributions of soot produced in laboratory flames[6,9,10] and to determine (qualitatively) temporal and spatial distributions of soot formation during diesel engine combustion.[11-15] Many of these studies have been performed with the assumption that the integrated signal following the laser pulse is independent of laser fluence at fluences above some threshold value. Given this assumption, attenuation of the laser beam through the sample (by scattering and absorption) can be ignored as long as the fluence remains above the threshold value. Recent studies have shown, however, that this assumption is not always valid, and the conditions under which it is valid are not well understood. [5,7,10,16-19] Furthermore, current LII models are inadequate for predicting LII signals and unable to reproduce particle temperatures throughout the heating and cooling process and thus cannot help establish the validity of the technique.[20-22]

To test current models and investigate the influence of experimental conditions on LII behavior, we have measured time-resolved LII signals from soot in a nonsmoking coflow ethylene diffusion flame over a wide range of laser fluences.[22] To facilitate comparisons with models, a Nd:YAG laser with a pulse duration of 7 ns was injection seeded, which provided a smooth laser temporal profile, and the beam was passed through an aperture and relay-imaged into the flame, which provided a smooth laser spatial profile. LII temporal profiles were recorded with a fast photodiode with adequate temporal resolution to capture signal evolution

during the laser pulse. We used these results to aid in the development of a model that predicts the temporal behavior of LII from soot on a nanosecond time scale. The model accounts for particle heating by laser absorption, oxidation, and annealing and cooling by sublimation, conduction, and radiation. The model also includes mechanisms for convective heat and mass transfer, melting, and nonthermal photodesorption of carbon clusters.[21]

A second set of experiments was performed to investigate the fast photodesorption mechanism in more detail. In these experiments the particles were heated with pulses of ~70 ps duration from a regeneratively amplified modelocked Nd:YAG laser. The signal was imaged onto one side of the slit of a streak camera and collected over the wavelength range 590-900 nm. Elastic Laser Scatter (ELS) was collected simultaneously on each laser shot on the other side of the slit. Using this arrangement we have collected data from an atmospheric laminar ethylene coflow diffusion flame to fluences as high as 0.3 J/cm^2 with a temporal resolution of ~65 ps.

Parameters to which the model is sensitive include the initial soot temperature, the temperature of the ambient gas, and the partial pressure of oxygen. In order to narrow the model uncertainties, we have developed a source of soot that allows us to determine and control these parameters. Soot produced by a burner is extracted, diluted, and cooled in a flow tube, which is equipped with a Scanning Mobility Particle Sizer (SMPS) for characterization of the aggregates.

LII temporal profile measurements

Methodology

Soot was generated in a nonsmoking laminar diffusion flame with a visible flame height of 2.9-4.1 cm. The flame was produced by a burner with a central fuel nozzle surrounded by a honeycomb region for the coflow of air and stabilized by a 38-cm-high shield surrounding the burner, focusing optics, and detector. Typical flow conditions were in the range of 0.065-0.085 standard liters per minute (SLM) of ethylene and 10-20 SLM of air. We have varied the fuel, burner dimensions, and flow rates to test the sensitivity of the technique to different conditions.

Particle-heating rates are nonlinearly dependent on laser fluence, and detailed analysis of the LII signals requires smooth temporal and spatial profiles from the laser used to heat the particles. A smooth temporal profile was achieved with an injection-seeded Nd:YAG laser, the second harmonic of which produced pulses at 532 nm with a pulse duration of ~7 ns full width at half max (FWHM) and repetition rate of 10 Hz. A smooth spatial profile was achieved by passing the beam through a ~1-mm aperture, which was relay imaged to the vertical centerline of the flame with a 1:1 telescope.

The laser beam was sent through the upper region of the flame 1.8-2.1 cm above the burner. The signal from the center portion of the flame was imaged onto a fast silicon photodiode with a rise time of <300 ps. A long-wave pass filter (>570 nm) was used in front of the detector to block laser scatter and emission from electronically excited C_2, and broadband emission was collected over 570-1100 nm. A 1064-nm notch filter was used to block scatter from any residual of the fundamental laser beam. The signal was collected on an oscilloscope with a 3-GHz bandwidth. Profiles were collected for laser fluences in the range of 0.01-1.00 J/cm^2. More details about these experiments are given in Ref. 22.

Similar experiments were performed to investigate fast processes that occur in the first few nanoseconds of excitation. These experiments used the second harmonic (532 nm) output of a regeneratively amplified cw modelocked Nd:YAG laser with a 70-ps pulse duration and

repetition rate of 20 Hz. A ~2.5-mm aperture was placed in the beam, and a 2:1 telescope was used to reduce the beam size and relay image the aperture into the flame. The signal was imaged onto one side of the slit of a streak camera and collected over the wavelength range 590-900 nm. Elastic Laser Scatter (ELS) is collected simultaneously on each laser shot on the other side of the slit. Using this arrangement, we have collected data from an atmospheric laminar ethylene coflow diffusion flame to fluences as high as 0.3 J/cm^2 with a temporal resolution of ~65 ps.

Results

LII temporal profiles recorded with the nanosecond system are shown for selected laser fluences in Figure 1. The signal depends on the particle diameter ($\propto D^3$) and temperature ($\propto \sim T^5$). As the particle temperature increases during the laser pulse, the signal increases, and the particle cools and shrinks (from carbon cluster sublimation and photodesorption), the signal decreases. At laser fluences below ~0.2 J/cm^2, temperatures increase rapidly during the laser pulse and slowly decay (on microsecond timescales) following the laser pulse. This slow decay is predominantly due to conductive cooling.[8, 9, 20-24] At higher fluences particles quickly reach and surpass the sublimation temperature of ~4000 K, becoming superheated, and then cool via sublimation back to the sublimation point.[8, 9, 20-22, 24-27] Sublimation also causes particles to decrease in size. At higher fluences, decay rates during and just after the laser pulse are fast, which may be largely attributable to photodesorption of carbon clusters.[21, 22] Annealing to more ordered forms of carbon may influence heating, cooling, and mass loss rates at nearly all fluences.[21, 22]

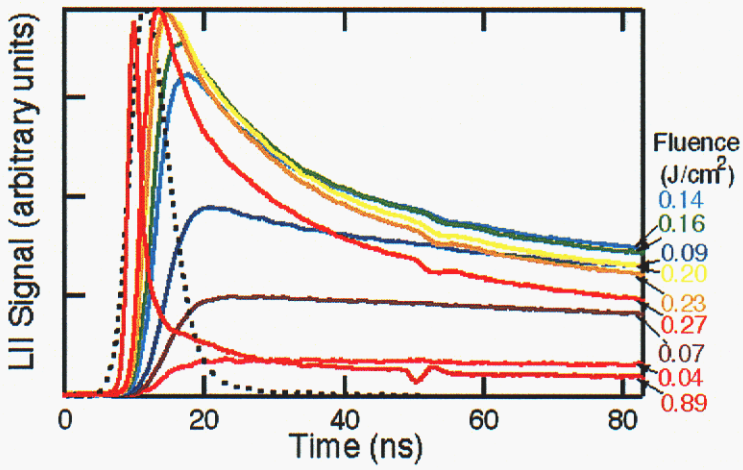

Figure 1. LII temporal profiles from the nanosecond experiment. LII temporal profiles (solid lines) are shown for selected laser fluences. Particles were heated with a laser with a pulse duration of ~7 ns, and signal was collected on a fast Si photodiode with a rise time of <300 ps. The laser temporal profile is indicated by the dotted line.

Figure 2 shows LII temporal profiles collected with the picosecond system at fluences similar to those associated with the LII data in Figure 1. Although the timescales differ by nearly a factor of 100 between the nanosecond experiments and the picosecond experiments, the LII signals demonstrate very similar temporal behavior relative to the laser pulse. This similarity in behavior at fluences above 0.2 J/cm^2 supports a fast mechanism for cooling and mass loss at these fluences. This set of experiments will allow us to isolate mechanisms that take place on

short timescales (e.g., absorption, nonthermal photolytic desorption) from processes that are predicted to evolve over longer (nanosecond) timescales (e.g., thermal sublimation, annealing).

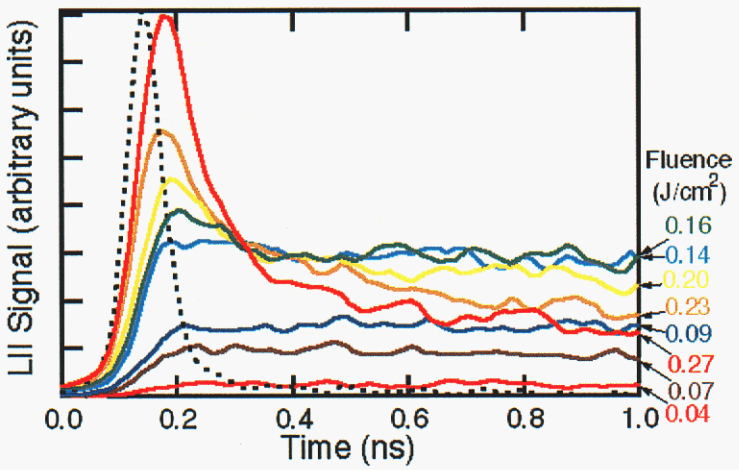

Figure 2. LII temporal profiles from the picosecond experiment. LII temporal profiles (solid lines) are shown for selected laser fluences. Particles were heated with a laser with a pulse duration of ~70 ps, and signal was collected on a streak camera at a temporal resolution of ~65 ps. The laser temporal profile is indicated by the dotted line.

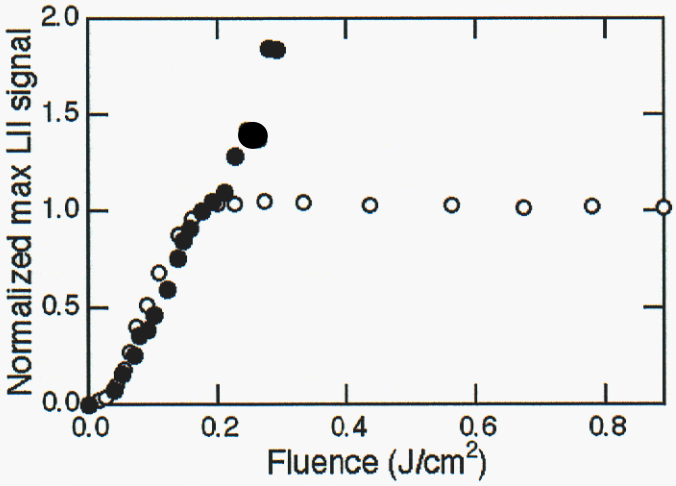

Figure 3. Fluence dependence of the peak LII signal. The maximum of the temporal profile is shown as a function of laser fluence. Results from the nanosecond experiments are represented by open circles, and those from the picosecond experiments are represented by filled circles. Results are normalized to 1 at 0.175 J/cm^2.

Figure 3 shows the effects of laser fluence on the magnitude of the LII signal. At fluences below 0.2 J/cm^2, the results of both the nanosecond and picosecond experiments demonstrate an increase in the maximum signal with increasing laser fluence. In the nanosecond experiment, the maximum signal is independent of fluence above 0.2 J/cm^2, whereas the maximum signal in the picosecond experiment continues to increase at these fluences. The lack of fluence dependence demonstrated in the nanosecond experiments may be attributable to considerable mass loss from photodesorption during the laser pulse; a reduction in the size of the particle during the laser pulse would limit absorption.[21, 22] Such a mechanism, however, might not be fast enough to occur during a 70-ps laser pulse, which could explain the different behavior between the two experiments.

LII model

Methodology

Models typically used to describe LII are based on a model initially developed by Melton in which energy- and mass-balance equations are solved to account for particle heating by laser absorption and cooling by conduction to the surrounding atmosphere, radiative emission, and sublimation. Particle size reduction during sublimation is also calculated. LII signal is derived from calculated temperatures and sizes using the Planck function weighted by the emissivity and the detector's wavelength response. The Melton model[24] uses (1) temperature-independent values for density and specific heat to determine the internal energy of the particle, (2) a Rayleigh approximation to calculate laser absorption and radiative emission rates, (3) the approximation of kinetic control of C_3 only from the surface to calculate sublimation rates, (4) a thermal accommodation coefficient and heat capacity associated with temperatures near room temperature, and (5) a formulation for conductive cooling appropriate for a transition regime between Knudsen and continuum flow.

We have developed a model[21, 22] that similarly solves the energy- and mass-balance equations but also includes (1) temperature-dependent thermodynamic parameters for calculating sublimation, conduction, and internal energy storage by the particle, (2) wavelength-dependent optical parameters to describe absorption and emission of radiation based on a Rayleigh-Debye-Gans approximation to account for aggregation, (3) convective heat and mass flow (Stefan flow) during the sublimation of multiple cluster species (C, C_2, C_3, C_4, and C_5) from the surface, (4) a thermal accommodation coefficient appropriate for high temperature conductive cooling, (5) a conductive cooling mechanism assuming free molecular flow at low pressure and a transition regime at high pressure, (6) nonthermal photodesorption resulting in loss of heat and mass by carbon clusters leaving the particle, (7) phase changes (i.e., annealing and melting) and their effects on absorption, radiation, sublimation, and photodesorption, and (8) oxidative heating at the particle surface.

The model descriptions of cooling and mass loss by sublimation and photodesorption are the most important terms for calculating the temporal behavior and magnitude of the LII signal at fluences above 0.2 J/cm^2. This part of the model is also the most complex and, in the case of photodesorption, the most uncertain. Although previous studies have suggested that laser photodesorption of carbon clusters from graphite can proceed by a nonthermal mechanism,[28-33] the nature of this mechanism, including the number of photons required, is not known. Our model includes such a mechanism assuming that it proceeds via a 2-photon process at 532 nm with a cross section and enthalpy of reaction approximated by comparing the results with the data.

Soot particles anneal into multi-shell carbon onions at temperatures above ~2500 K when heated in a furnace or by a laser,[34-38] and graphite surfaces have been shown to melt at atmospheric pressure when heated rapidly with a laser.[39-42] Changes in the phase of soot primary particles are likely to influence heating and cooling rates because of differences in physical properties, such as the index of refraction, enthalpies and entropies of formation of carbon clusters, and thermal accommodation coefficients. Soot annealing rates have not been measured under the conditions encountered during laser heating on sub-second timescales; we infer these rates from annealing rates measured on graphite at lower temperatures on longer timescales. Annealing rates are calculated in the new model using an Arrhenius expression with activation

energies for interstitial migration and vacancy/defect formation derived from studies of graphitization. Full details of the new model are given in Ref. 21.

Results

Figure 4 shows a comparison of results from the new model with results from the nanosecond experiments. This figure also includes results from the Melton model,[24] the model on which many current LII models are based. The maximum values have been scaled to agree in order to facilitate comparison of the shapes of the temporal profiles. Both the measurements and the model results demonstrate a steep rise in LII signal as the particles heat and slower decay in LII signal as the particles cool. At fluences in the range 0.15-0.3 J/cm^2, however, the new model overpredicts the LII decay rate during and immediately following the laser pulse, whereas at fluences of 0.3-0.7 J/cm^2, the new model underpredicts the early decay rate. Similar discrepancies are seen for the Melton model. The Melton model more severely overpredicts the LII decay rate at all fluences below 0.4 J/cm^2 and underpredicts the decay rate at higher fluences.

At low fluences, the differences between the two models are largely due to the thermal accommodation coefficients used to calculate the conductive cooling rate. The Melton model uses a value (0.9) that is appropriate for low-temperature conditions, whereas the new model uses a value (0.3) derived from measurements made on graphite at temperatures of 700-1400 K. Discrepancies between the models are also partially attributable to differences in the treatment of conductive cooling; the new model assumes free molecular flow conditions when the mean free path exceeds the particle diameter by a factor of ~7, whereas the Melton model assumes that the system is always in the transition regime between Knudsen and continuum flow. Free molecular flow is appropriate when the primary particles are assumed to have minimal contact, i.e., when aggregation is neglected. Both models neglect aggregation for the conduction calculation, which is predicted to decrease conductive cooling rates via the shielding effect. Calculations using quasi-Monte Carlo algorithms indicate that accounting for aggregation would reduce the conductive cooling rate by ~30% for an aggregate of 500 primary particles and a thermal accommodation coefficient of 0.3.[43]

At higher fluences, the new model gives better agreement with the measurements mainly because (1) at intermediate fluences annealing reduces the rate of cooling by sublimation and (2) at higher fluences photodesorption increases the mass and heat loss rate (and therefore signal decay rate) during the laser pulse. At these fluences, the differences between the two models are also apparent in the predicted fluence dependence of the magnitude of the signal, as shown in Figure 5. Including the nonthermal photolysis term allows the new model to reproduce the lack of fluence dependence of the peak signal at fluences above 0.2 J/cm^2, whereas the Melton model predicts that the signal continues to increase with fluence. Neither model has been run for conditions relevant to the picosecond experiment.

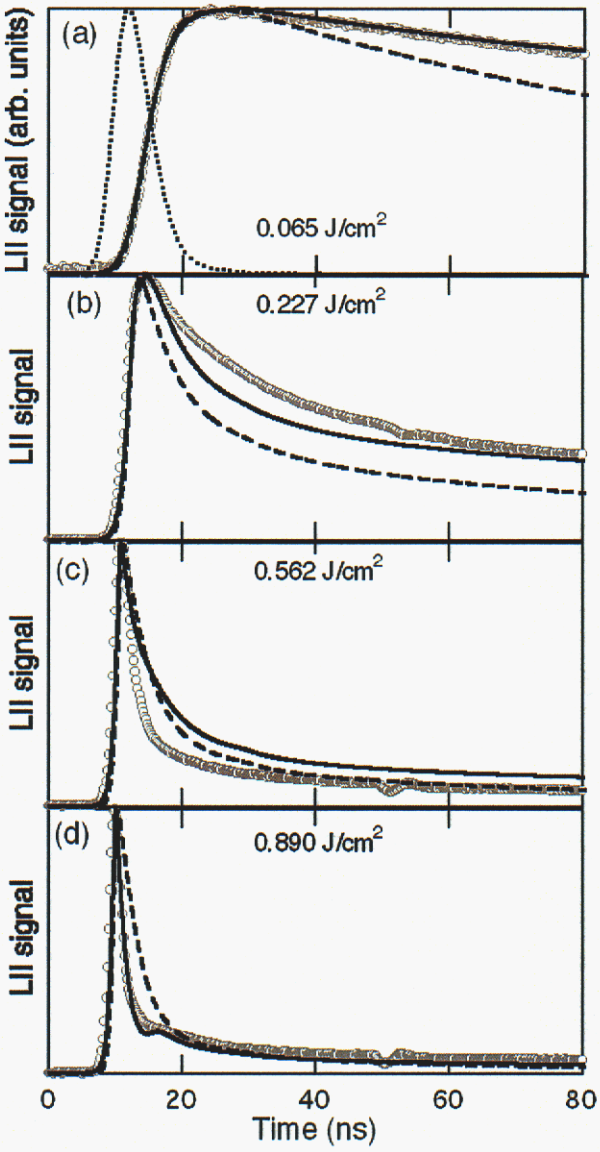

Figure 4. Comparison of model results with measured LII temporal profiles. Profiles are shown for selected fluences, as noted in each panel. Measurements are shown for the nanosecond experiments (circles). The results of the Melton model are represented by dashed lines, and those from the new model are depicted by solid lines. In each panel the maximum of the modeled and measured temporal profiles are normalized to the same value. The dotted curve in (a) shows the measured laser temporal profile.

Despite the improved agreement between modeled and measured signals with the new model over previous models, lingering discrepancies demonstrated at intermediate and high fluences suggest an incomplete understanding of the mechanisms for sublimation, photodesorption, and annealing. Experimental uncertainties in the mean fluence (~5%) cannot explain the inability of the models to reproduce these observations, and other mechanisms, such as conductive cooling, have little effect at these fluences. Uncertainties related to the treatment of sublimation in the models are large and include those associated with (1) neglecting aggregation, which may lower sublimation rates and (2) assuming thermodynamic properties of graphite. In addition, the photodesorption mechanism is speculative, and the uncertainties associated with it are

substantial. The annealing process and the influence it has on sublimation and photodesorption are also very poorly understood.

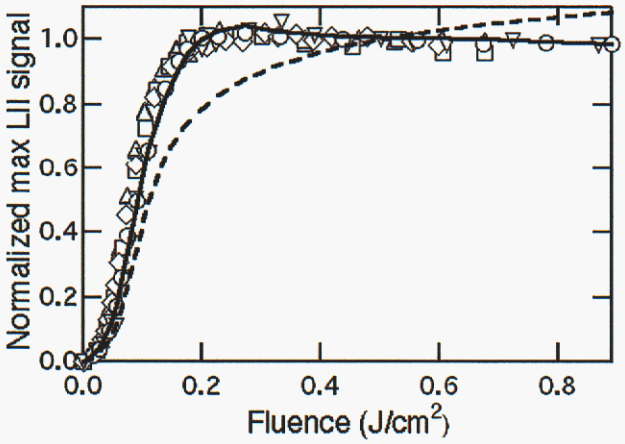

Figure 5. Comparison of model results with measured LII fluence dependence. The maximum of the temporal profile is shown as a function of laser fluence. Results from the nanosecond experiments (circles) are compared with results from the new model (solid line) and the Melton model (dashed line). Results are normalized to 1 at 0.2 J/cm^2.

Exhaust simulator

Uncertainties in the model input lead to substantial uncertainties in the model results. Parameters to which the model is sensitive include the initial soot temperature, the temperature of the ambient gas, and the partial pressure of oxygen. In order to narrow the model uncertainties, we have developed a source of soot that allows us to determine and control the ambient environment. We initially investigated the viability of using aspirated lampblack as a surrogate for combustion-generated soot. This source, however, demonstrated problems with solvent condensation when characterized with the Scanning Mobility Particle Sizer (SMPS) and did not produce a stable carbon aerosol concentration over time. Ablation of a graphite surface to generate sub-micron carbon particle posed similar stability problems.

In our current design, shown in Figure 6, soot is generated by a coflow laminar diffusion flame, which is intercepted by a cross flow of N_2 to extract, dilute, and cool the soot as it travels down a flow tube. Using this soot source, we are able to investigate the cooling rate of the particles as a function of the temperature of the surrounding air, which will allow us to infer a thermal accommodation coefficient for air. We are also able to study the influence of the initial temperature of the soot on the rise time and peak signal. In addition, we can control the composition of the ambient atmosphere, and, by changing the O_2 partial pressure, we will be able to investigate the effect of oxidation on the cooling rate.

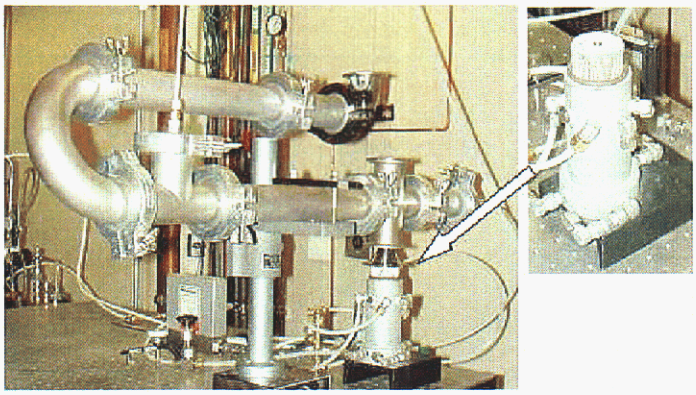

Figure 6. Photograph of the exhaust simulator. The exhaust simulator uses a cross flow of air to break the tip of a coflow diffusion flame. The burner used to generate the particles is shown in the inset.

This apparatus also allows us to control particle size distributions by selection of fuel and flow conditions of the flame. Soot aggregate size is monitored by an SMPS attached to the flow tube. Figure 7 shows size distributions measured with the SMPS for two flow conditions.

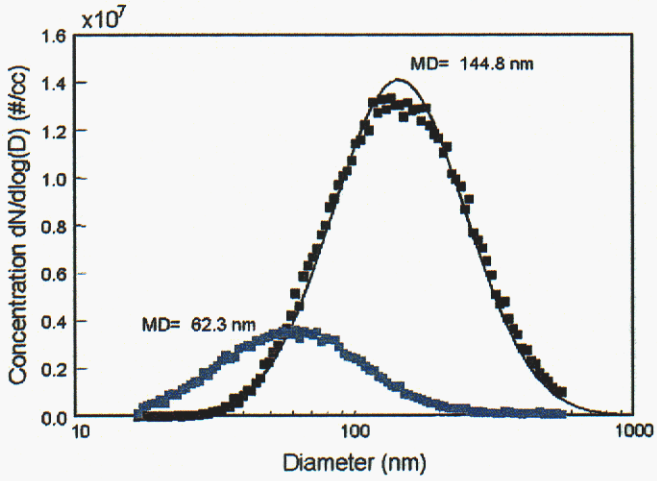

Figure 7. Exhaust simulator aggregate size distributions. Symbols show SMPS measurements of aggregate size distributions recorded at two locations in the flow tube of the soot source, and curves represent Gaussian fits to the data. Higher fuel flow rates (black squares) give larger mean diameters than lower fuel flow rates (gray squares).

Summary

We have recorded time-resolved LII signals from an ethylene diffusion flame over a wide range of laser fluences. We have performed these experiments using an injection-seeded Nd:YAG laser with a pulse duration of 7 ns and a regeneratively amplified modelocked Nd:YAG laser with a pulse duration of 70 ps. Both experiments used the second harmonic at 532 nm. The detector response time for the former setup was 300 ps, and the temporal resolution of the latter was ~65 ps.

In order to test the validity of LII under varying environmental conditions, we have developed a model that describes the heating of soot particles during the laser pulse and the subsequent cooling of the particles by radiative emission, sublimation, and conduction. The model additionally includes particle heating by oxidation, accounts for the likelihood of particle annealing, and incorporates a mechanism for nonthermal photodesorption. We have compared

the LII temporal profiles from the nanosecond experiments with results from the new model and from the Melton model,[24] i.e., the model on which most currently used LII models are based. The new model reproduces the temporal behavior and relative magnitudes at low fluences (0.15 J/cm^2), whereas the Melton model overpredicts the conductive cooling and signal decay rates at these fluences. Both models demonstrate discrepancies with the observations at intermediate (0.15-0.3 J/cm^2) and higher (0.3-0.7 J/cm^2) fluences, suggesting an incomplete understanding of the sublimation process. Although both models overpredict the LII signal decay rate at intermediate fluences, the new model includes a mechanism for annealing, which decreases the decay rate in this fluence range, and thus provides better agreement with the measurements. Both models underpredict the decay rate at higher fluences. Inclusion of a photodesorption mechanism for heat and mass loss allows the new model to reproduce the LII decay rate at high fluences (>0.7 J/cm^2) and the relative magnitude of the peak signal as a function of fluence, which are not reproduced by the Melton model. The models have not been tested under conditions relevant to the picosecond experiments.

Parameters to which the model is sensitive include the initial soot temperature, the temperature of the ambient gas, and the partial pressure of oxygen. In order to narrow the model uncertainties, we have developed a source of soot that allows us to determine and control these parameters. Soot produced by a burner is extracted, diluted, and cooled in a flow tube, which is equipped with a Scanning Mobility Particle Sizer (SMPS) for characterization of the aggregates.

References

1. D. B. Kittelson, "Engines and nanoparticles: A review," J. Aerosol Sci. 29(5/6), 575-588 (1998).
2. Health Effects Institute, "Airborne particles and health: HEI epidemiologic evidence" Cambridge, MA, 2001.
3. H. Horvath, "Aerosols: An introduction," J. Environ. Radioact. 51, 5-25 (2000).
4. IPCC, *Climate Change 2001: The Scientific Basis. Contribution of Working Group I to the Third Assessment Report of the Intergovernmental Panel on Climate Change* (Cambridge University Press, Cambridge, UK and New York, NY, 2001).
5. T. Ni, J. A. Pinson, S. Gupta, and R. J. Santoro, "Two-dimensional imaging of soot volume fraction by the use of laser-induced incandescence," Appl. Opt. 34, 7083-7091 (1995).
6. R. L. Vander Wal and D. L. Dietrich, "Laser-induced incandescence applied to droplet combustion," Appl. Opt. 34(6), 1103-1107 (1995).
7. C. R. Shaddix and K. C. Smyth, "Laser-induced incandescence measurements of soot production in steady and flickering methane, propane, and ethylene diffusion flames," Combust. Flame 107, 418-452 (1996).
8. B. Mewes and J. M. Seitzman, "Soot volume fraction and particle size measurements with laser-induced incandescence," Appl. Opt. 36, 709-717 (1997).
9. N. P. Tait and D. A. Greenhalgh, "PLIF imaging of fuel fraction in practical devices and LII imaging of soot," Ber. Bunsenges. Phys. Chem. 97, 1619-1625 (1993).
10. R. L. Vander Wal and K. J. Weiland, "Laser-induced incandescence: Development and characterization towards a measurement of soot volume fraction," Appl. Phys. B: Lasers Opt. 59, 445-452 (1994).
11. J. E. Dec, A. O. zur Loye, and D. L. Siebers, "Soot distribution in a D. I. diesel engine using 2-D laser-induced incandescence imaging," Proc. SAE, SAE Paper No. 910224 (1991).
12. J. A. Pinson, D. L. Mitchell, and R. J. Santoro, "Quantitative, planar soot measurements in a D. I. diesel engine using laser-induced incandescence and light scattering," Proc. SAE, SAE Paper No. 932650 (1993).

13. C. Espey and J. E. Dec, "Diesel engine combustion studies in a newly designed optical-access engine using high speed visualization and 2-D laser imaging," Proc. SAE, SAE paper no. 930971 (1993).
14. K. Inagaki, S. Takasu, and K. Nakakita, "In-cylinder quantitative soot concentration measurement by laser-induced incandescence," Proc. SAE, SAE Paper No. 1999010508 (1999).
15. B. Axelsson and P. O. Witze, "Qualitative laser-induced incandescence measurements of particulate emissions during transient operation of a TDI diesel engine," Proc. SAE, SAE Paper no. 2001-2001-3574 (2001).
16. R. L. Vander Wal and K. A. Jensen, "Laser-induced incandescence: Excitation intensity," Appl. Opt. 37, 1607-1616 (1998).
17. P.-E. Bengtsson and M. Aldén, "Soot-visualization strategies using laser techniques," Appl. Phys. B: Lasers Opt. 60, 51-59 (1995).
18. C. R. Shaddix and K. C. Smyth, "Quantitative measurements of enhanced soot production in steady and flickering methane/air diffusion flames," Combust. Flame 99, 723-732 (1994).
19. B. Quay, T.-W. Lee, T. Ni, and R. J. Santoro, "Spatially resolved measurements of soot volume fraction using laser-induced incandescence," Combust. Flame 97, 384-392 (1994).
20. S. Schraml, S. Dankers, K. Bader, S. Will, and A. Leipertz, "Soot temperature measurements and implications for time-resolved laser-induced incandescence (TIRE-LII)," Combust. Flame 120, 439-450 (2000).
21. H. A. Michelsen, "Understanding and predicting the temporal response of laser-induced incandescence from carbonaceous particles," J. Chem. Phys. 118(15), 7012-7045 (2003).
22. H. A. Michelsen, P. O. Witze, D. Kayes, and S. Hochgreb, "Time-resolved laser-induced incandescence of soot: The influence of experimental factors and microphysical mechanisms," Appl. Opt. 42, 5577-5590 (2003).
23. S. Will, S. Schraml, and A. Leipertz, "Two-dimensional soot-particle sizing by time-resolved laser-induced incandescence," Opt. Lett. 20, 2342-2344 (1995).
24. L. A. Melton, "Soot diagnostics based on laser heating," Appl. Opt. 23, 2201-2208 (1984).
25. P. O. Witze, S. Hochgreb, D. Kayes, H. A. Michelsen, and C. R. Shaddix, "Time-resolved laser-induced incandescence and laser elastic scattering measurements in a propane diffusion flame," Appl. Opt. 40, 2443-2452 (2001).
26. A. C. Eckbreth, "Effects of laser-modulated particulate incandescence on Raman scattering diagnostics," J. Appl. Phys. 48, 4473-4479 (1977).
27. S. Will, S. Schraml, K. Bader, and A. Leipertz, "Performance characteristics of soot primary particle size measurements by time-resolved laser-induced incandescence," Appl. Opt. 37, 5647-5658 (1998).
28. D. J. Krajnovich, "Laser sputtering of highly oriented pyrolytic graphite at 248 nm," J. Chem. Phys. 102, 726-743 (1995).
29. K. A. Lincoln and M. A. Covington, "Dynamic sampling of laser-induced vapor plumes by mass spectrometry," Int. J. Mass Spectrom. Ion Phys. 16, 191-208 (1975).
30. R. W. Dreyfus, R. Kelly, and R. E. Walkup, "Laser-induced fluorescence study of laser sputtering of graphite," Nucl. Instrum. Methods Phys. Res. B23, 557-561 (1987).
31. P. T. Murray and D. T. Peeler, "Dynamics of graphite photoablation: Kinetic energy of the precursors to diamond-like carbon," Appl. Surf. Sci 69, 225-230 (1993).
32. F. Kokai, K. Takahashi, M. Yudasaka, and S. Iijima, "Emission imaging spectroscopic and shadowgraphic studies on the growth dynamics of graphitic carbon particles synthesized by CO_2 laser vaporization," J. Phys. Chem. B 103, 8686-8693 (1999).
33. E. A. Rohlfing, "Optical emission studies of atomic, molecular, and particulate carbon produced from a laser vaporization cluster source," J. Chem. Phys. 89, 6103-6112 (1988).

34. R. L. Vander Wal, T. M. Ticich, and A. B. Stephens, "Optical and microscopy investigations of soot structure alterations by laser-induced incandescence," Appl. Phys. B: Lasers Opt. 67, 115-123 (1998).
35. R. L. Vander Wal and M. Y. Choi, "Pulsed laser heating of soot: Morphological changes," Carbon 37, 231-239 (1999).
36. D. Ugarte, "High-temperature behaviour of "fullerene black"," Carbon 32, 1245-1248 (1994).
37. M. Miki-Yoshida, R. Castillo, S. Ramos, L. Rendón, S. Tehuacanero, B. S. Zou, and M. José-Yacamán, "High resolution electron microscopy studies in carbon soots," Carbon 32, 231-246 (1994).
38. W. A. de Heer and D. Ugarte, "Carbon onions produced by heat treatment of carbon soot and their relation to the 217.5 nm interstellar absorption feature," Chem. Phys. Lett. 207, 480-486 (1993).
39. T. Venkatesan, D. C. Jacobson, J. M. Gibson, B. S. Elman, G. Braunstein, M. S. Dresselhaus, and G. Dresselhaus, "Measurement of thermodynamic parameters of graphite by pulsed-laser melting and ion channeling," Phys. Rev. Lett. 53, 360-363 (1984).
40. A. M. Malvezzi, "Picosecond laser heating and melting of graphite," Int. J. Thermophys. 11, 797-809 (1990).
41. J. Heremans, C. H. Olk, G. L. Eesley, J. Steinbeck, and G. Dresselhaus, "Observation of metallic conductivity in liquid carbon," Phys. Rev. Lett. 60, 452-455 (1988).
42. M. Balooch, M. Schildbach, R. Tench, M. Allen, and W. J. Siekhaus, "Surface site specificity on the basal plane of graphite: 1.06 μm laser damage threshold and reactivity with oxygen between 350 and 2300 K," J. Vac. Sci. Technol. B 9, 1088-1091 (1991).
43. A. V. Filippov, M. Zurita, and D. E. Rosner, "Fractal-like aggregates: Relation between morphology and physical properties," J. Colloid Interface Sci. 229, 261-273 (2000).

Distribution

1 MS 9054 W. J. McLean, 8300
1 MS 9054 R. W. Carling, 8350
1 MS 9056 W. L. Hsu, 8356
1 MS 9054 D. R. Hardesty, 8360
1 MS 9053 D. L. Siebers, 8362

3	MS 9018	Central Technical Files, 8945-1
1	MS 0899	Technical Library, 9616
1	MS 9021	Classification Office, 8511/Technical Library, MS 0899, 9616 DOE/OSTI via URL
1	MS 0188	D. Chavez, LDRD Office, 1030